

# The Cu induced ultraflat band in the room-temperature superconductor $\text{Pb}_{10-x}\text{Cu}_x(\text{PO}_4)_6\text{O}_4$ ( $x=0,0.5$ )

Kun Tao\*, Rongrong Chen, Lei Yang, Jin Gao, Desheng Xue and Chenglong Jia

Key Lab for Magnetism and Magnetic Materials of Ministry of Education, Lanzhou University,  
730000 Lanzhou, China

([taokun@lzu.edu.cn](mailto:taokun@lzu.edu.cn))

Based on the first principle calculations, we investigate the geometry and the electronic structures of the room temperature superconductor lead apatite with and without the Cu doped. Our calculations found that without the Cu doping the lead apatite crystal is an insulator with a flat band above the Fermi level. Furthermore, our results indicate that by introducing the  $\text{O}_1$  vacancies would results in the disappear of the flat bands in the undoped crystal. While the Cu is doped forming the LK-99, there exist the ultra-flat bands crossing the Fermi level induced by the doped Cu atoms, which is due to the hybridization between the d states of the Cu atoms and the p states of the fully occupied  $1/4$  occupied  $\text{O}_1$  atoms. Moreover, we point out that the hybridization maybe the key for the realization of the room temperature superconductivity for the LK-99, and a possible solutions method to improve the quality of the superconductivity is proposed. Our work provides a foundation for the future studies on the unique electronic and the superconductivity properties of the LK-99 crystal.

Being the holy grail of condensed matter physics, the high- $T_c$  superconductors due to their unique characteristics of zero resistance and perfect diamagnetism [1] with huge potential applications for an energy-efficient future and are used in a billion-dollars market. Milestones of superconductivity research include its discovery by Onnes in 1911, the BCS theory of Bardeen, Cooper and Schrieffer [2], and the discovery of high- $T_c$  superconductors by Bednorz and Müller [3], and more recently that of hydride superconductors by Eremets and coworkers [4] and the subsequently followed by several new classes including the Fe-pnictides in 2008 [5] and as well as nickelate superconductivity by Li et al. [6]. Moreover, twisted bilayer graphene [7,8]

with the flat bands near the Fermi level, which is a signal of the superconductivity have been discovered. Strong correlation bands are a common feature of many high  $T_c$  superconducting families, which will generate unconventional mechanisms for Cooper pair formation. Strong correlation bands are a common feature of many high  $T_c$  superconducting families, which will bring about new unconventional mechanisms that arise.

Finding a room-temperature superconductor has been the ultimate dream for the condensed matter physicist. However, a definitive roadmap to achieving room temperature  $T_c$  under ambient pressures is still remained elusive. While the recently claimed in a nitrogen-doped lutetium hydride [9] at near-ambient pressure superconductivity still remains a subject of ongoing

debate[10-13]. However, it was recently reported by Lee et al. [14,15] who proclaim that they have successfully synthesized even at the ambient pressure such a room temperature superconductor,  $\text{Pb}_{10-x}\text{Cu}_x(\text{PO}_4)_6\text{O}$  with  $0.9 < x < 1$ . The recipe to synthesize  $\text{Pb}_{10-x}\text{Cu}_x(\text{PO}_4)_6\text{O}$  appears quite easy for other groups are also easy to follow up with[16-18]. Thus further experiments will reveal whether  $\text{Pb}_9\text{Cu}(\text{PO}_4)_6\text{O}$  is indeed the first room-temperature superconductor or not. Nevertheless, it is exiting and a definitely call for a more thorough theoretical understanding of this rather unusual material[19-22].

In the paper, we performed the first principle calculations to investigate the geometrical and the electronic structure of the lead apatite. With carefully analyzing of the geometry and the electronic structure of the before and after the Cu doped lead apatite, we point out that the hybridization between the d states of the Cu atoms and the p states of the fully occupied 1/4 occupied O1 atoms determines the quality of the superconductivity of the LK-99. And based on our calculations, we proposed a possible solution method to improve the quality of the LK-99.

Our calculations are performed in the framework of Density Functional Theory (DFT) as implemented in the Vienna Ab initio Simulation Package (VASP) package [23,24] with the projector augmented wave (PAW) potentials. The basis set contained plane waves with a kinetic energy cutoff of 520 eV and the total energy was converged to 10<sup>-6</sup> eV. The Brillouin zone integration is carried out with 4\*4\*4 k-pointing sampling for undoped structures and with a Gamma-pointing sampling for the Cu

doped structures of a 2\*2 supercell of the  $\text{Pb}_{10-x}\text{Cu}_x(\text{PO}_4)_6\text{O}$  with  $x=0, 0.5$ . All geometries were optimized without any symmetry constraint until all residual forces on each atom were less than 0.01 eV/Å. And the width of the Gaussian smearing for the density of states calculations are set to be 0.05 eV.

The structure of the  $\text{Pb}_{10}(\text{PO}_4)_6\text{O}$  is presented in Figs. 1. The structure possesses P63/m symmetry (space group no. 176) with a hexagonal lattice. Here we consider the lead apatite. Taking its structure reported from X-ray diffraction in Ref. [25] and from COD (Crystallography Open Database) data of the pure lead-apatite as the parent compound. The lattice constants are optimized with the VASP code with the ionic positions, cell volume, and cell shape are all allowed to change. The optimized lattice are  $a=b=10.16575$  Å and  $c=7.36679$  Å, in good agreement with the experimental values  $a=9.865$  Å and  $c=7.431$  Å. The predicted larger lattice parameters may arise from the overestimation of the employed PBE functional, Here, should point out that with our relaxed lattice constant, we plotted the band structure and found that it only has little difference with that obtained from the experimental lattice constant, see supplementary. Therefore, in the following calculations we used the experimental lattice constant for all calculations.

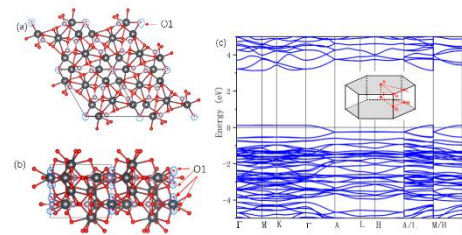


Fig 1. The top view (a) and the side

view and (b) of the crystal structure of lead-apatite with a chemical formula  $(\text{Pb}_{10}(\text{PO}_4)_6\text{O}_4)$  that used in our calculations. respectively. The atoms circled in blue are the  $\text{O}_1$  atoms. (c) The calculated band structure of the lead apatite. The inset in (b) shows the high symmetry k-points selected for plotting the band structure in (a).

We noticed that in the lead-apatite, there exists two symmetry inequivalent Pb atoms, named  $\text{Pb}_1$  and  $\text{Pb}_2$ , and the  $\text{Pb}_1$  atoms form a hexagon, while the  $\text{Pb}_2$  atoms form two oppositely shaped triangles. We also notice that the  $\text{O}_1$  atoms are 1/4 occupied, as it is not part of the six  $\text{PO}_4$  tetrahedron, which are marked with the blue circles, as shown in the Fig.1(a), (b). As for our calculations, we used a fully occupied  $\text{O}_1$  atoms which are 1/4 occupied in the literature, that is the reason why our formula of the lead apatite  $(\text{Pb}_{10}(\text{PO}_4)_6\text{O}_4)$  is different with the formula  $\text{Pb}_{10}(\text{PO}_4)_6\text{O}$  in the reported papers. And the other  $\text{O}_2$  atoms which form the six  $\text{PO}_4$  tetrahedrons. We should point out that these two types of the O atoms are inequivalent. The calculated electronic band structure of the lead apatite is shown in the Fig.1 (c). It can be observed from the Fig 1(c) that there exist an ultraflat band along the Gamma-M-K-Gamma and also A-L-H-A path, and the corresponding band width is near 0.24 meV and the 2 meV, as shown in the supplementary. And there is also an indirect band gap of about 2.72 eV between the Gamma point and the middle point along the Gamma-M path. The obtained insulating nature of lead apatite is consistent with the experimental observations [33,34].

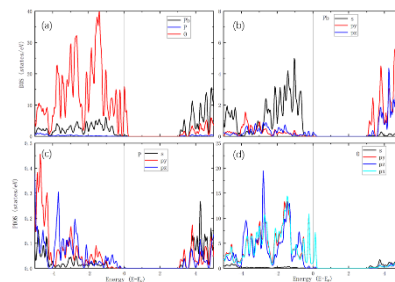


Fig.2 The calculated density-of-states of the lead apatite. (a) The sum of all Pb, P and O atoms. (b), (c) and (d) The projected density of states for the Pb, the P and the O atoms, respectively.

There is a peak just located at the Fermi level which is mainly caused by the hybridization between the O  $p_y(p_x)$  and the Pb  $p_z$  orbitals, as shown in the Fig 2(a), which results in an ultraflat band just about 0.126 eV above the Fermi level, as shown in the Fig 3 (a). Full occupied  $\text{O}_1$  atoms are very important, which results in a metal, as shown in the Fig 3 (b). With a further investigation on the two types of the O atoms, it can be found from the Fig.3 (a) that the  $\text{O}_1$  atoms give the vital contributions to the flat band. It means that the fully occupied  $\text{O}_1$  atoms reported in the literature determines the flat band. Or in other words, since the  $\text{O}_1$  atoms are only 1/4 occupied, the  $\text{O}_1$  vacancies determines whether the flat bands exist or not.

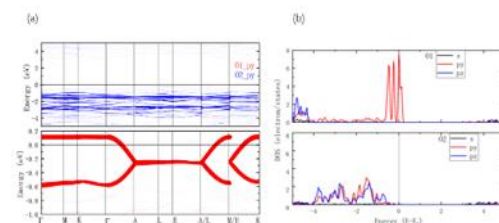


Fig.3 (a) The projected band structure for the  $\text{O}_1$  and the  $\text{O}_2$  atoms. (b) The projected density-of-states for the  $\text{O}_1$

and the O<sub>2</sub> atoms, respectively.

In order to check our assumption right or not, we removed three out of four O<sub>1</sub> atoms in calculations forming the Pb<sub>10</sub>(PO<sub>4</sub>)<sub>6</sub>O structure as reported by the experiments. The band structure is plotted in the Fig 4 (a). It can be observed that the flat bands disappear. Because the bond length between the Pb1 atoms with that of the O1 atoms change from the 2.58 Å to 2.27 Å, such strong local distortion will result in the disappear of the flat band. And a nearly flat band with the band width of about 0.11 eV can be observed but below the Fermi level about 0.25 eV along the A-L-H-A path, as shown in the Fig 4 (a). It is due to the hybridization between the Pb p orbitals and the O p<sub>y</sub> (p<sub>x</sub>) orbitals. With a further observation of the projected bands for the O<sub>2</sub> and the O<sub>1</sub> atoms, as shown in the Fig 4 (d), it can be found that the flat band is mainly composed by the O<sub>1</sub> p<sub>y</sub> orbitals. Therefore, we may conclude that the O<sub>1</sub> vacancies determines the electronic structure of the undoped lead-apatite crystal.

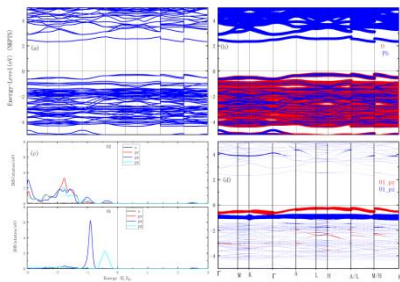


Fig.4 (a) The calculated band structure of the Pb<sub>10</sub>(PO<sub>4</sub>)<sub>6</sub>O with the O<sub>1</sub> vacancy after the fully relaxations. (b) The projected band structure on the O and the Pb atoms. The projected density of states (c) and the band structure on the O<sub>1</sub> and the O<sub>2</sub> atoms.

After analyzing structural and electronic properties of lead-apatite, we

turn to LK-99. We perform the calculations for the high-temperature nonmagnetic solution without taking into account the on-site Coulomb interactions for the Cu-3d shell. The LK-99 crystal in experiment has a chemical formula of Pb<sub>10-x</sub>Cu<sub>x</sub>(PO<sub>4</sub>)<sub>6</sub>O with 0.9 < x < 1.1 [34]. Furthermore, it was reported that the Cu atoms will occupy the Pb2 positions in the crystal structure [15]. In order to simulate the Cu substitute the Pb2 site, we use a 2\*2 supercell with two Pb2 atoms are replaced by two Cu atoms, resulting in Pb<sub>9.5</sub>Cu<sub>0.5</sub>(PO<sub>4</sub>)<sub>6</sub>O<sub>4</sub>, as shown in the Fig 4.

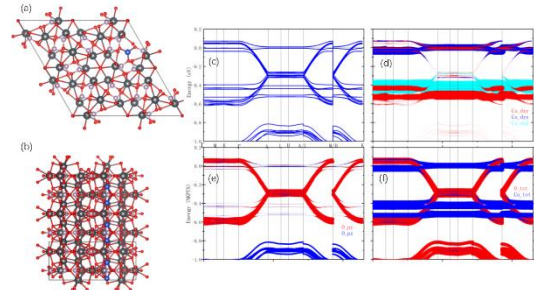


Fig.5 (a), (b) The top view and the side view of the crystal structure of the Cu doped lead apatite (Pb<sub>9.5</sub>Cu<sub>0.5</sub>(PO<sub>4</sub>)<sub>6</sub>O<sub>4</sub>). (c) The calculated band structure of the Pb<sub>9.5</sub>Cu<sub>0.5</sub>(PO<sub>4</sub>)<sub>6</sub>O<sub>4</sub> crystal. The projected band structure on the Cu atoms (d), O atoms (e) and the hybridization between the Cu and the O atoms.

Comparing with the Pb<sub>10</sub>(PO<sub>4</sub>)<sub>6</sub>O<sub>4</sub> crystal, it can be found that the doped Cu induced some extraordinary ultraflat bands just across the fermi level, as shown in the Fig 5 (c). These induced ultraflat band is mainly due to the hybridizations between the Cu atoms and the O atoms, as it can also be observed from the Fig 5 (f). With a carefully analyze of the projected bands and the density of states for the Cu atoms, as shown in the Fig 5 (d) and the Fig 6 (b), it can be found that these induced flat

bands can be attributed to the Cu  $d_{xz}(d_{yz})$  orbitals which just sit over the Fermi level. It can also be observed from the Fig 5 (a) and (b) that the Cu doped induced some lattice distortions. The bond length between the Pb1 and the O1 atoms changes from the 2.58 Å to the 2.73 Å, such a large increase in the Pb-O bond length will induce a strong local lattice distortion, which leads to the splitting of the O p orbitals into the  $p_x(p_y)$  and the  $p_z$  orbitals, as shown in the Fig.5 (e) and Fig.6 (d).

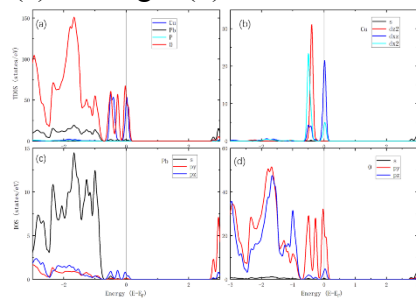


Fig.6. (a) The calculated density of states for the  $\text{Pb}_{9.5}\text{Cu}_{0.5}(\text{PO}_4)_6\text{O}_4$  crystal. The PDOS on the Cu (b), the Pb (c) and the O (d) atoms, respectively.

Since there are two types of the O atoms  $\text{O}_1$  and the  $\text{O}_2$ , as shown with different color in the Fig.7 (a) and (b), it should give further investigations on the contribution of each O atoms to the flat band. From the Fig 7 (c) and (d), it can be observed that there is a big difference in the contribution to the flat bands for the two types of the O atoms. The fully occupied of the 1/4 occupied  $\text{O}_1$  atoms give the vital contributions to the flat band, while that of the  $\text{O}_2$  atoms only give very small contributions to the flat band. Based on the above analysis we can obtain a conclusion that the  $\text{O}_1$  vacancy will have a vital effect on the electronic structure of the  $\text{Pb}_{10-x}\text{Cu}_x(\text{PO}_4)_6\text{O}_4$  crystal. Moreover, here a new model should be used to describe the physics of LK-99, unlike the widely studied one-

band Hubbard model applicable to cuprates [26,27], since the bands are contributed by the hybridization between the Cu  $3d_{xz}(d_{yz})$  and the  $d_{xy}(d_{x^2-y^2})$  states with its next next nearest-neighboring O1 atoms  $p_y(p_x)$  states. In comparison with to the non-doped lead-apatite, Cu doping results in an insulator-metal transition which was claimed as one of the key factors contributing to the realization of room-temperature superconductivity in LK-99 [15].

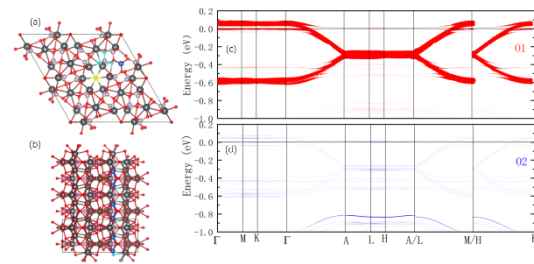


Fig.7 (a), (b) The top view and the side view of the crystal structure of the  $\text{Cu Pb}_{9.5}\text{Cu}_{0.5}(\text{PO}_4)_6\text{O}_4$ . The atoms in yellow are the  $\text{O}_1$  atoms and that in blue are the  $\text{O}_2$  atoms, respectively. The corresponding Pband on the  $\text{O}_1$  (c) and the  $\text{O}_2$  (d) atoms.

Based on the above discussions, we may conclude that the hybridization between the Cu d-states of the Cu doped with the p state of the fully occupied 1/4 occupied  $\text{O}_1$  atoms may be the key for the realization of the room temperature superconductivity. In order to improve the quality of the superconductivity caused by  $\text{O}_1$  vacancy, we suggest annealing in oxygen atmosphere as reported in the CuO nanostructures with the postannealing in the different O atmosphere the O vacancy decreased enormously. And we believe that with such annealing under the oxygen atmosphere the quality of the superconductivity should be greatly improved.



In summary, we performed the first principle calculations to investigate the electronic structure of the LK-99, and we found that the hybridizations between the Cu doped atoms and the fully occupied 1/4 occupied O1 atoms determines the quality of the LK-99 in the superconductivity. Based on our calculations, a possible solutions method to improve the quality of the superconductivity is proposed.

The authors thank Daqiang Gao for fruitful discussion. This work was supported by the National Natural Science Foundation of China (Nos. 12174164, 91963201, and 11834005) and the 111 Project under Grant No. B2006. This work was carried out at National Supercomputer Center in Tianjin, and the calculations were performed on Tianhe new generation supercomputer.

- [1] P. Mangin and R. Kahn, *Superconductivity: An introduction* (Springer Cham, New York, 2016).
- [2] J. Bardeen, L. N. Cooper, and J. R. Schrieffer, *Phys.Rev.* 106, 162 (1957).
- [3] J. G. Bednorz and K. A. Müller, *Zeitschrift für Physik B Condensed Matter* 64, 189 (1986).
- [4] A. P. Drozdov, M. I. Erements, I. A. Troyan, V. Ksenofontov, and S. I. Shylin, *Nature* 525, 73 (2015).
- [5] Y. Kamihara, T. Watanabe, M. Hirano, and H. Hosono, *Journal of the American Chemical Society* 130, 3296 (2008).
- [6] D. Li, K. Lee, B. Y. Wang, M. Osada, S. Crossley, H. R. Lee, Y. Cui, Y. Hikita, and H. Y. Hwang, *Nature* 572, 624 (2019).
- [7] Cao, Y.; Fatemi, V.; Demir, A.; Fang, S.; Tomarken, S. L.; Luo, J. Y.; Sanchez-Yamagishi, J. D.; Watanabe, K.; Taniguchi, T.; Kaxiras, E.; Ashoori, R. C.; Jarillo-Herrero, P. *Nature* 2018, 556, 80–84.
- [8] Cao, Y.; Fatemi, V.; Fang, S.; Watanabe, K.; Taniguchi, T.; Kaxiras, E.; Jarillo-Herrero, P. *Nature* 2018, 556, 43–50.
- [9] N. Dasenbrock-Gammon, E. Snider, R. McBride, H. Pasan, D. Durkee, N. Khalvashi-Sutter, S. Munasinghe, S. E. Dissanayake, K. V. Lawler, A. Salamat, and R. P. Dias, *Nature* 615, 244 (2023).
- [10] X. Ming, Y.-J. Zhang, X. Zhu, Q. Li, C. He, Y. Liu, T. Huang, G. Liu, B. Zheng, H. Yang, J. Sun, X. Xi, and H.-H. Wen, *Nature* (2023), 10.1038/s41586-023-06162-w.
- [11] X. Xing, C. Wang, L. Yu, J. Xu, C. Zhang, M. Zhang, S. Huang, X. Zhang, B. Yang, X. Chen, Y. Zhang, J. gang Guo, Z. Shi, Y. Ma, C. Chen, and X. Liu, arXiv:2303.17587 (2023).
- [12] N. P. Salke, A. C. Mark, M. Ahart, and R. J. Hemley, arXiv:2306.06301 (2023).
- [13] D. Peng, Q. Zeng, F. Lan, Z. Xing, Y. Ding, and H. kwang Mao, arXiv:2307.00201 (2023).
- [14] S. Lee, J.-H. Kim, and Y.-W. Kwon, arXiv:2307.12008 (2023).
- [15] S. Lee, J. Kim, H.-T. Kim, S. Im, S. An, and K. H. Auh, arXiv:2307.12037 (2023).
- [17] Hao Wu, Li Yang, Bichen Xiao, Haixin Chang, arXiv:2308.01516 (2023).
- [18] P. Abramian, A. Kuzanyan, V. Nikoghosyan, S. Teknowijoyo, and A. Gulian, arXiv: 2308.01723(2023).
- [19] Sin'ead M. Griffin, arXiv:2307.16892v1(2023)
- [20] G. Baskaran, arXiv:2308.01307 (2023)
- [21] Junwen Lai, Jiangxu Li, Peitao Liu, Yan Sun, and Xing-Qiu Chen, arXiv:2307.16040

- [22] Liang Si and Karsten Held, arxiv: 2308.00676
- [23] G. Kresse and J. Hafner, Phys. Rev. B: Condens. Matter Mater. Phys., 1993, 47, 558.
- [24] G. Kresse and J. Furthmuller, Phys. Rev. B: Condens. Matter Mater. Phys., 1996, 54, 11169.
- [25] Krivovichev, S.V.; Burns, P.C, Zeitschrift fuer Kristallographie (149,1979-), 2003, 218, 357-365
- [26] E. Gull and A. J. Millis, Nature Physics 11, 808 (2015).
- [27] H.-C. Jiang and T. P. Devereaux, Science 365, 1424 (2019).